Thermochemical conversion of solid digestates: Effects of temperature and fluidizing gas on products composition

Mohamed Hechmi Aissaoui, Jasmine Hertzog, Cecilia Sambusiti, Paola Gauthier-Maradei, Marie-Noëlle Pons, Vincent Carré, Yann Le Brech, Anthony Dufour

Journal of Analytical and Applied Pyrolysis 186 (2025) 106928

Contents lists available at ScienceDirect

Journal of Analytical and Applied Pyrolysis

journal homepage: www.elsevier.com/locate/jaap

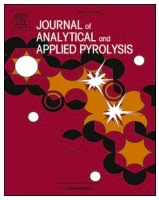

Thermochemical conversion of solid digestates: Effects of temperature and fluidizing gas on products composition

Mohamed Hechmi Aissaoui [a], Jasmine Hertzog [b], Cecilia Sambusiti [c], Paola Gauthier-Maradei [d], Marie-Noëlle Pons [a], Vincent Carré [b], Yann Le Brech [a], Anthony Dufour [a,*]

[a] Université de Lorraine, CNRS, LRGP, 1 rue Grandville, Nancy 54000, France
[b] Université de Lorraine, LCP-A2MC, Metz 57000, France
[c] TotalEnergies, CSTJF, Centre Scientifique et Technique Jean Féger, Av. Larribau, Pau 64000, France
[d] TotalEnergies, Centre de Recherche de Solaize (CRES), Chem. du Canal, Solaize 69360, France

ARTICLE INFO

Keywords:
Digestate
Micro-fluidized bed
Pyrolysis
Gasification

ABSTRACT

Valorizing digestates from methanisation plants through their thermochemical conversion is an important topic. For this purpose, a micro-fluidized bed reactor was operated by varying the reactor temperatures (from 400 °C to 900 °C) and the fluidizing gas (nitrogen, steam or air). All experiments were conducted by keeping a constant fluidization regime (U/U_{mF}= 2.5) and gas-phase residence time in the freeboard (1.2 s). The mass yields of solids (char and ashes), syngas, and liquids (bio-oils or tar) were quantified. The importance of dehydration and decarboxylation reactions on char composition is highlighted by the Van Krevelen diagram. The effect of steam on N/C composition of char is also discussed. Gas composition was analyzed by chromatography, FTIR (for HCN), and spectrophotometry (for NH_3). NH_3 is the major N-gas species for all conditions. Its formation is promoted by steam. It is not significantly converted under our conditions even at 900 °C. HCN is an important product increasing from 700 °C and notably at 900 °C. The liquids were analyzed by GC/MS and high-resolution mass spectrometry (Fourier-transform ion cyclotron resonance, FT-ICR MS). Principal component analysis of FT-ICR MS data unravels the effect of air and steam on the composition of liquid products. Air promotes the formation of CHNO species whereas steam does not significantly impact the composition of the liquids (compared to pyrolysis) on the whole range of temperatures. At 900 °C, all liquids present a similar composition (based on FT-ICRMS analysis) highlighting the predominant effect of temperature over the reactive gas at 900 °C.

1. Introduction

Several waste processing technologies, such as biological (i.e., anaerobic digestion, composting, fermentation, …) and thermochemical (i.e., pyrolysis, gasification, combustion, and hydrothermal processes) have been developed to valorize wastes into energy and/or value-added products.

Anaerobic digestion (AD) is a biological process that converts organic biomasses into biogas and digestate, a valuable amendment and fertilizer [1]. Due to this dual interest, the number of AD plants has been quickly rising worldwide in recent years. Digestate treatments may be required before its final disposal in some cases depending on digestate composition[2], country regulations and disposal costs [3].

At industrial scale, the composition of digestate is not always compatible with land spreading because of residual greenhouse gas (GHG) emissions [4,5], logistic and regulation reasons. Therefore, other valorization routes are explored [2], like thermochemical processes to produce energy[6] and/or high value-added products [7]. In recent years, some reviews have focused on coupling biological and thermochemical processes [1,3,4,7,8] and most of the studies concerned digestates pyrolysis and gasification processes.

"Slow" digestate pyrolysis was mainly assessed at lab-scale in "spoon" (or tubular) or fixed bed reactors, under slow heating rates (about 5–10 K/min) to promote char production with final temperature between 350 °C and 800 °C [6,9–18] and a solid residence time at the final temperature ranged between 10 min and 240 min (more often at 60 min).

Most of studies have been devoted solely to the characterization of pyrolysis chars [12–18]. Funke et al.[19] presents an interesting study on the effect of water during the pyrolysis of digestates. They showed

* Corresponding author.
E-mail addresses: mohamed-hechmi.aissaoui@univ-lorraine.fr (M.H. Aissaoui), anthony.dufour@univ-lorraine.fr (A. Dufour).

https://doi.org/10.1016/j.jaap.2024.106928
Received 28 July 2024; Received in revised form 28 November 2024; Accepted 18 December 2024
Available online 19 December 2024

that steam thermal carbonization allows for a higher solid content (solid biomass mass (dry basis) per total mass of feedstock) in the reactor because the biomass is subjected to saturated steam instead of liquid water. The carbon losses in the liquid phase are decreased and less water needs to be heated up during carbonization.

Wei et al. [20] valorized digestate through slow pyrolysis at 5 K/min at different final temperatures (350 °C to 550 °C) and pressures (atmosphere to 8 MPa) for 20 min. Karaeva et al. [6] provides a qualitative analysis of the bio-oil produced from the pyrolysis of digestate. They show that bio-oil was mainly composed of acetic acid (at 550 °C, 10 K/min, based on GC/MS area, not quantitative). Tayibi et al. [9] pyrolyzed anaerobic solid digestate coming from anaerobic digestion of wastewater sludge and quinoa residues at 500 °C for 1 h (at 10 K/min) in a fixed bed (300 g of biomass). The biochar obtained was compatible with soil applications as amendment [21]. The organic phase of the bio-oil had a HHV of 34 MJ/kg and a high carbon content of 70.6 wt%. Monlau et al. [11] carried out pyrolysis experiments using a quartz rotary kiln reactor. The maximum yield of the bio-oil was obtained at 500 °C and it ranged between 53.0–58.4 wt%, pyrolysis gas ranged from 8.8–11.3 wt%, and 32.8 –35.7 wt% for biochar. The bio-oil was composed by 58 wt% C, 5 wt% H, 34 wt% O and 1 wt% N.

The work of Hornung et al. [10] is specific because it involves a secondary reactor for gas reforming (over a hot char bed as a catalyst for tar reforming). This technology promotes tar reforming and H_2 production. It presents a complete characterization of liquids (elemental analysis, HHV, total acid number, water content). The bio-oil had a carbon content higher than 79 wt% and a HHV higher than 35 MJ/kg. The gas composition from digestates pyrolysis was presented in several studies [9,10,22–24]. In all the studies, the major gas (in %vol.) is CO_2 at 500 °C (produced by decarboxylation reactions). Then, H_2 and CO are promoted at higher reactor temperatures by secondary conversion of primary tar (mainly cracking and decarbonylation reactions). All results on gas composition were presented in vol%. They are not relevant to discuss the formation of gas: molar (or mass) yields (mol or g gas/g biomass) are required to discuss gas formation [25]. To the best of our knowledge, there is no work dealing with a detailed and quantitative characterization of the molecular species present in digestate bio-oils as-produced by fast pyrolysis (e.g., in a fluidized bed). Moreover, the residence time of gas-phase in the hot zone (one of the main factor controlling gas composition [25]) was never provided for all reviewed articles. Therefore, the formation of gas and bio-oils cannot be assessed with these studies.

Few studies concerned digestate gasification or combustion. Chen et al. [26] have studied the gasification of digestates from a biogas plant at temperatures ranging from 600 °C to 800 °C in a batch fixed bed and as a function of the equivalence ratio (ER). They have included a characterization of ashes (by XRF and proximate analysis). They found an optimum in the cold gas efficiency (CGE, defined in supplementary material) of 67 % at 0.28 ER (800 °C). Obviously, the increase in the bed temperature promotes the production of H_2 and CO.

The gasification of digestates has been also studied by Balas et al. [27] in a pilot fluidized bed of 100 kW (~40 kg/h biomass). They have compared digestates from wet and dry fermentation for various temperatures (730–760 °C) and ER. They have also quantified the main monoaromatic compounds (benzene, xylenes, others) but not heavier tar components such as polyaromatic hydrocarbons (PAHs). The CGE was between 66 % and 74 %. The CGE and syngas yields were not optimal due to the low temperatures of gasification which were limited by the sintering of the ashes. Kratzeisen et al. [28] studied the combustion of digestates pellets in a pilot combustion facility. They concluded that the calorific value, the ash properties and the emissions allow their use in the investigated combustion unit but further investigations are required to cover a broader range of digestates and combustion techniques.

Despite all these extensive studies, we did not find research articles dealing with the fast pyrolysis of solid digestates in a fluidized bed. There is still a lack of knowledge in bio-oil composition from digestates pyrolysis. Furthermore, and to the best of our knowledge, there is no study comparing the mass yields in products for pyrolysis, gasification and combustion on the same digestate, same reactor and under comparable conditions (with a constant gas-phase residence time).

Consequently, the novelty of this work lies on the 3 following points:

1) A solid digestate has been converted in a fluidized bed under pyrolysis (N_2), gasification (H_2O/N_2) and combustion (air) conditions;
2) Mass yields in main products are provided for a large range of temperatures (400–900°C) with a constant gas-phase residence time of volatiles in the free-board;
3) The liquid products (bio-oils and tars) are characterized by GC/MS and high-resolution mass spectrometry (FT-ICR MS) for the first time.

2. Material and methods

In this work, a solid digestate (SD) produced from the anaerobic digestion in a biogas territorial plant was converted in a micro-fluidized bed reactor. The main conditions and products characterization methods are summarized in Fig. 1.

2.1. Origin of solid digestate and pretreatment

The solid digestate was sampled at a collective biogas plant fed with 30 wt% agro-industrial residues, 50 wt% of silage maize residues, 20 wt % of manure, after a solid and liquid separation step by screw pressing. The digestate sample was stored at −20 °C before the drying and pelletisation step. 500 g of the wet solid digestate was dried at 40 °C during 24 h. Then, the dried digestate was crushed with a knife crusher at 1500 round/min with a mesh of 2 mm. Pellets were produced from dried and crushed digestates to reduce the elutriation of fine particles during pyrolysis experiments in the fluidized bed. Elutriation reduces biomass conversion and leads to plugging issues at the outlet of the reactor. Pellets were prepared by a manual press with a diameter of 6 mm and a final thickness of 4 mm.

2.2. Micro fluidized bed reactor

The fast pyrolysis, partial combustion and steam gasification processes were conducted and compared by using a micro fluidized bed (Fig. 2) performed at the same temperature range (400 – 900 °C), fluidization velocity (2.5 U/U_{mF}, U for gas velocity and U_{mF} for minimum fluidization gas velocity) and gas phase residence time (1.2 s).

A custom-made quartz-based furnace was used to heat the fluidized bed. It allows to visualize the fluidization [29] during the pyrolysis (for temperatures lower than 600 °C). This design is of interest to identify potential segregation or agglomeration behaviors of the fluidized bed in real-time and in hot conditions. The reactor (2 cm I.D., 12 cm length) was filled with 20 g of Fontainebleau sand (150 μm – 300 μm). The sand was preheated to the target process temperature (between 400 °C and 900 °C) under the flow of carrier gas: N_2 for pyrolysis, air for combustion and, 80 %vol. of H_2O and 20 % vol. of N_2 for gasification. The flow rate of the carrier gas was adjusted as a function of the reactor temperature to keep a constant fluidization velocity (U) (and therefore a constant gas-phase residence time) of 10 cm/s corresponding to 2.5 U/UmF. The minimal fluidization velocity (UmF) of the sand bed was measured at

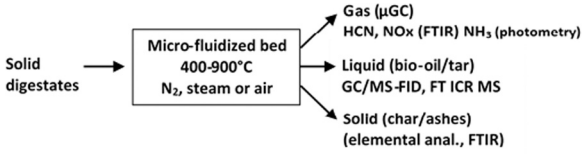

Fig. 1. Experimental methods used in this work.

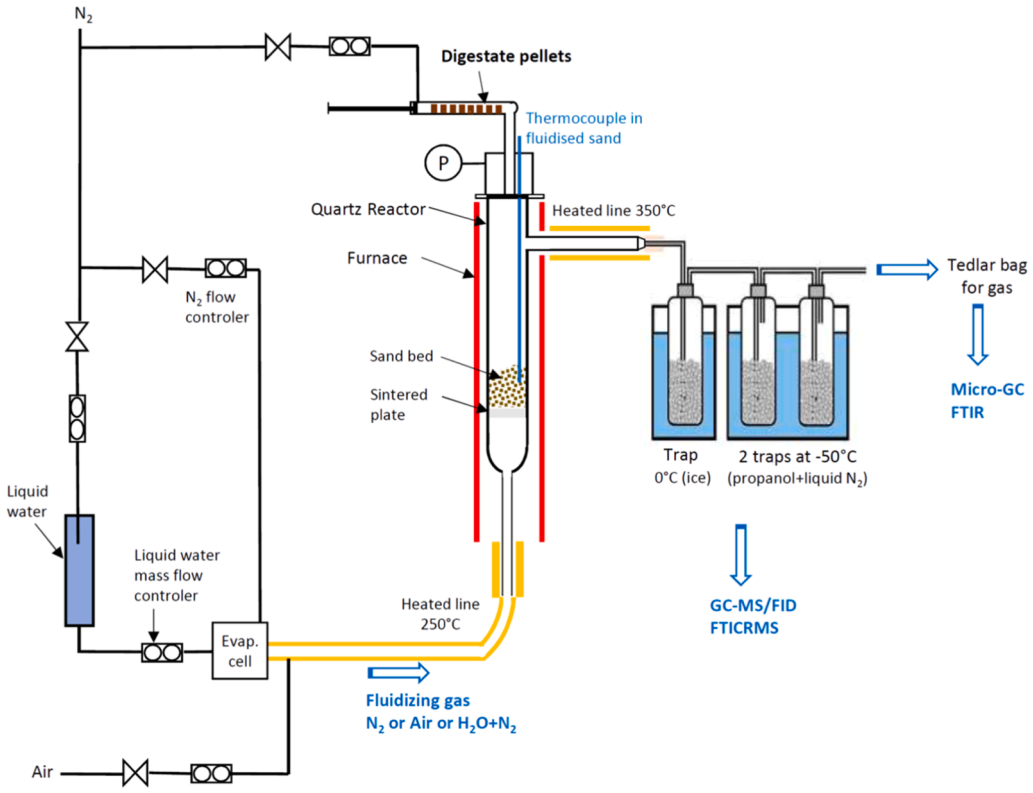

Fig. 2. Micro fluidized bed reactor used for fast pyrolysis (N_2), combustion (air) and steam gasification (80 %vol. of steam and 20 % vol. of N_2) processes of pelletized solid digestate.

4 cm/s in excellent agreement with Xu et al. [30].

1 g of solid digestate (dried, crushed and pelletized) was injected in the preheated fluidized bed during 5 min. The gas-phase residence time in the freeboard was kept constant at 1.2 s for all conditions. The gas-phase residence time was as short as 0.15 s in the heated line (350 °C) between the freeboard outlet and the entrance of the first cold trap.

For the steam gasification process, the liquid water flow rate was controlled by a Coriflow controler (Bronkhorst) and the liquid was vaporized in a Controlled Evaporater Mixer (CEM) (Bronkhorst) entrained by N_2.

Experiments were conducted with air as fluidization gas for partial combustion. The corresponding equivalence ratio calculation is provided in supplementary material.

At the reactor outlet, the vapors were condensed in 3 cold traps: a first one immersed in ice-water (0 °C), and the 2 other ones immersed in a solution at −50 °C, prepared by a mix of liquid N_2 and isopropanol. Quartz balls were positioned in the cold traps to break the aerosols and to improve the cooling surface for the steam. The 3 traps were weighted before and after the experiment to quantify the mass of liquid fraction ("bio-oil" for pyrolysis, including water). In the following text, "liquid" stands for all the condensable species sampled in the cold traps. The traps were then rinsed with methanol (MeOH). The condensed liquids collected in the 3 traps were diluted in 20 mL of MeOH (total volume). The entire gas flow exiting the 3 cold traps was sampled in a Tedlar bag and further analysed. At the end of the experiment, the reactor was cooled down in N_2. The whole sand and solid residue (char and/or ashes) was weighted to quantify the mass of the solid residue. Char was collected (if not oxidized) and its elemental composition was determined.

2.3. Analytical methods

2.3.1. Analysis of the liquid

1 µL of tetradecene (internal standard) was spiked in the whole condensed liquid and MeOH solution (20 mL). The solution was then analyzed by GC/MS-FID on an Agilent 7890 A coupled to Agilent 5975 C TAD (TripleAxis detector) mass spectrometer and FID detector (in parallel of the MS). MS was operated at 70 eV electron impact. 1 µL of the solution was injected with a split ratio of 10 in a column Agilent HP-5MS (diphenyl 5 %, dimethylolysiloxane 95 %, 30 m length, 250 µm diameter, 0,25 µm thickness of the coated material). The GC furnace program was: 50 °C during 5 min, then 5 K/min up to 270 °C, then 270 °C during 15 min. The "de Saint-Laumer" et al. method [31] was used to quantify (on the FID) the molecules elucidated on the MS (by NIST database comparison).

Liquids were also characterized by ultra high-resolution Fourier transform ion cyclotron resonance mass spectrometry (FT-ICR MS 7 T, SolariX 2xR, Bruker Daltonics, Bremen, Germany) in positive-detection electrospray ionization (ESI - Bruker Daltonics). Each stock solution was diluted by 100 in methanol containing 0.01 mg/mL sodium acetate [32] and each liquid sample was analyzed in triplicate. Mass spectra were acquired over a 107.5 – 1500 m/z range, with a 4 megaword time-domain, and resulted from the accumulation of 300 scans. A mass resolution of 450,000 was achieved at m/z 300. More details regarding the analysis parameters, as well as the data treatment, assignment, and representations are given in supplementary material.

Perseus software was used to perform principal component analysis (PCA) of the assigned m/z taking into account their intensities in the ESI (+) FT-ICR mass spectra of the different liquid samples. The research profiles diagram was used to extract the molecular features specific to each conversion temperature.

2.3.2. Gas characterization

The gases were sampled after the cold traps in a Tedlar bag and then analyzed by micro-gas chromatography (SRA Instruments MicroGC 3000) and Fourier Transform InfraRed gas analyzer (FTIR) within less than 30 minutes after the end of the thermochemical experiment. A FTIR (Thermo Scientific Antaris) equipped with a Mercure Cadmium Tellure (MCT) photoelectric detector was used to identify and quantify HCN and NOx. The accuracy of this method was assessed by Kwapinska et al. [33]. The optical path length was 10 m and the volume of the cell 0.2 L. The cell was operated under vacuum and was heated to reduce the background signal and potential deposit. More details about the calibration method can be found in our previous work [34]. The gas present in the Tedlar bag at atmospheric pressure was injected in the cell by a controlled procedure. FTIR calibrations were obtained by injecting standards (from standard bottles provided by Air Liquide). To the best of our knowledge, we present the first report on N-species quantifications from digestates thermochemical conversion. We have checked that the cold traps did not impact the sampling and quantification of HCN (by FTIR) by conducting a separate experiment with traps at room temperature. The quantification of HCN was the same for traps at −50 °C or room temperature, therefore the cold traps (at −50 °C) do not absorb or condense HCN.

NH_3 gas analysis was carried out using the Nessler spectrophotometer method. Separate experiments were conducted for NH_3 quantification because uncontrolled NH_3 absorption occurred in the cold traps used for bio-oils analysis (for GC/MS and FT ICR MS analysis).Therefore the gases (heating line at 350 °C) from pyrolysis, steam gasification and combustion were directly passed through three cold impingers (at 0°C) each containing 35 mL of 0.1 N H_2SO_4 solution to absorb NH_3 [33]. All the connection lines were rinsed with 95 mL of this solution (leading to a total collected solution of 200 mL). 1 mL was sampled and diluted 100 times with ultrapure water. Ten milliliters of the diluted solution were filtered through a 0.45 μm syringe filter into a vial. Next, mineral stabilizer and polyvinyl alcohol (PVA) dispersing agent were added, followed by 400 μl of Nessler reagent. The results were read on a Hach spectrometer (calibrated for 0.1–2.0 mg/L NH_3). Furthermore, the whole procedure (sampling, rinsing, dilution and spectrophotometry) was checked by quantifying a known volume of NH_3 (controlled flowrate of a standard bottle and time of feeding) as sampled by the 3 impingers (with the same connection lines).

2.3.3. Char characterization

Elemental analysis was conducted in triplicate (RSD provided in table below) for solid digestates and all the char samples produced by "fast" pyrolysis and steam gasification using an Elementar Vario Cube. More details are provided in supplementary material on solids analysis.

FTIR Spectra were acquired using a Bruker Alpha FTIR in ATR mode between 4000 and 400 cm^{-1}. Water vapor subtraction was used where appropriate, and the baseline was corrected. Unscrambler V12.2 software was used for multivariate analysis. Principal component analysis (PCA) was used to analyze FT-IR imaging data in the 400–1600 cm^{-1} fingerprint spectral range.

Brunauer-Emmett-Teller (BET) specific surface area and pore volume of biochar (from pyrolysis and steam gasification produced at 600 °C to 900 °C) were determined by nitrogen sorption using Micromeritics 3Flex instrument. Prior the measurements, the samples were degassed overnight on sample ports at 620 K.

3. Results

3.1. Mass balances

Mass yields of products (i.e., gas, liquid and solid) were determined and compared for the 3 types of processes (i.e., fast pyrolysis, steam gasification and partial combustion) and for a broad range of reactor temperatures (400 °C to 900 °C). Results are presented in Fig. 3.

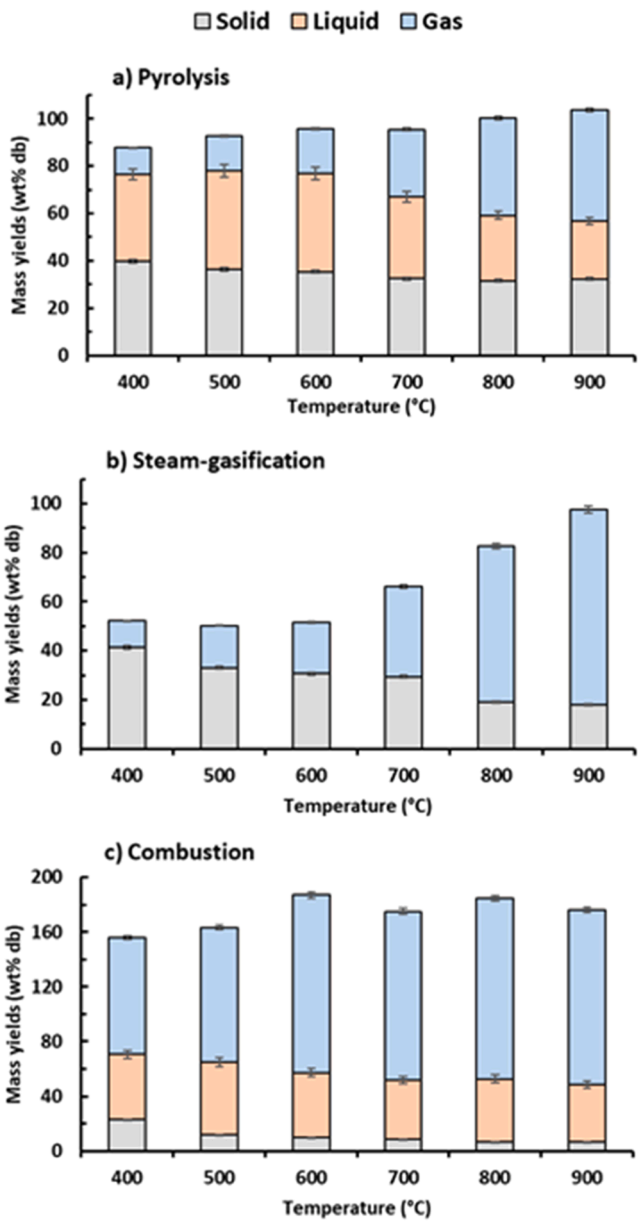

Fig. 3. Mass yields (wt% db) in solid products (char and ashes), liquids and gases as a function of the fluidized sand temperature and for different fluidizing gas (constant U/UmF and gas-phase residence time for all conditions): a) fast pyrolysis (N_2); b) steam gasification (80 vol% H_2O, 20 vol% N_2), c) partial combustion (air). It was not possible to quantify the mass of liquids for gasification conditions.

A good reproducibility on mass yields was observed (by triplicate experiments, see supporting material). The mass yield and relative standard deviations (RSD) at 500 °C for pyrolysis are: 36.4 wt% (1.2 wt % RSD) for biochar, 14.8 wt% (RSD 0.17 wt%) for gas and 41.5 wt% (RSD 2.1 wt%) for liquids (bio-oils).

Concerning pyrolysis, the mass balance closure ranges from 88 wt% (at 400 °C) to 104 wt% at 900 °C. It is under-estimated at the lower temperatures probably due to heavy liquid species deposited on the reactor wall. It was not possible to weight this small mass of deposit on the reactor. Mass balance is slightly over-estimated at 900 °C probably due to the gas quantification method. For combustion, the mass yields can be higher than 100 wt% (based on the anhydrous mass of the digestate) due to the addition of consumed O_2 in the products.

As expected for fast pyrolysis (Fig. 3a), the bio-oil mass yield

increases slightly from 400 °C (36 wt%) to 600 °C (41 wt%) and then decreases until 900 °C (25 wt%.). It is well established that secondary gas-phase reactions occur from about 600 °C (with a gas residence time in the range of 1 s) leading to the conversion of the condensable products (organics in bio-oils) and to an increase in the gas phase products [25,35]. The gas mass yield increases up to 47 wt% at 900 °C. Gases are mainly formed by the secondary conversion of volatiles in the free-board of the fluidized bed from 500 °C, which is in agreement with literature data [25,36]. As for solid (char), its mass yield decreases from 40 wt% at 400 °C to 32 wt% at 700 °C. Then, it stays globally stable from 700 °C highlighting that the devolatilisation of char is weak after 700 °C.

Concerning gasification, Fig. 3b) depicts the mass yields of solid and gas products as a function of the fluidized sand temperature. It was not possible to weight accurately the liquid products considering the high amount of water used to fluidize the sand bed compared to the mass of liquid produced by the digestates. For this reason, the liquids produced during gasification are not discussed in the following section. We have kept the same reference with the mass of anhydrous digestate in order to compare the mass yields between all experiments (for pyrolysis, combustion and steam gasification). Steam is a co-reactant (with digestates) and it increases the mass yield in gas. The mass yield of gas increases from 11 % at 400 °C up to 79 % at 900 °C. Char yield is similar as pyrolysis test at 400 °C (41 wt%), then decreases to 18 wt% at 900 °C. One can notice that the char yield decreases quickly at 800 °C due to char gasification reactions. It should be noticed that for a residence time of char particles between 4 and 9 min (see supplementary material), the char gasification is not even completed at 900 °C. Indeed, the char yield (18 wt%) is higher than the ash content of the digestate (7.2 wt%, Table S1). This result is very consistent with the kinetic behavior of char reported by other authors during steam gasification notably for in fluidized bed reactors [37].

For partial combustion (Fig. 3c), the mass balance is higher than 100 wt%db because air is a co-reactant. The consumption of O_2 as a function of temperature ranges from 29 %wt. (of O_2 injected) at 400 °C to 55 % at 900 °C (see Table S2). It demonstrates the importance of oxidation reactions at temperatures as low as 400 °C. Air presents a clear effect on mass yields (compared to pyrolysis) by reducing char yield and increasing those of liquid (by water formation) and gas (by CO_2 formation) even at 400;°C. The solid mass yield remains constant from 800 °C (at 6.7 wt%) highlighting the complete oxidation of the char at a residence time between 4 and 9 min in the fluidized bed reactor.

3.2. Char characterization

The elemental analysis of char is presented in Table 1. The ash content is presented in supplementary material.

The devolatilisation of the char, from 400 °C to 900 °C during fast pyrolysis, leads to an increase in C content (Table 1) and to a decrease in H and N contents (due to volatiles formation). This fact is well established in the literature [38,39]. The S content in char increases with temperature in agreement with previous work [38] due to the high stability of S-moieties in char.

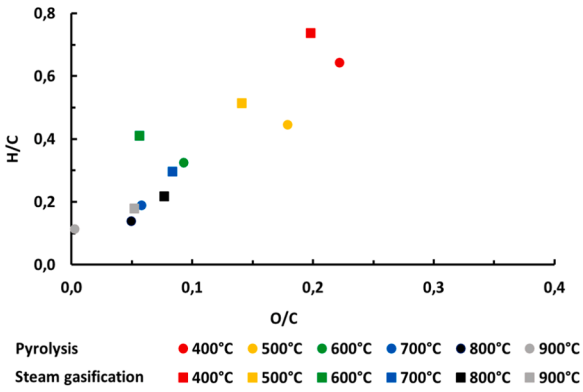

Fig. 4. Van Krevelen diagram (atomic H/C vs. atomic O/C) of the chars produced at different fluidized sand temperatures (fast pyrolysis and steam gasification).

The pyrolysis char produced at 400 °C represents 47 wt% of the initial carbon present in the digestate (49 wt% C see Table S1). At 900 °C, the char (yield 32 wt%db with 67.6 wt% C, see Table 1) still represents 45 wt% of the initial carbon of the digestate. Consequently, the devolatilisation between 400 °C and 900 °C only represents a very small fraction (2 wt%) of the initial carbon present in the digestate.

Concerning steam gasification, the carbon content of char increases from 59 wt% (400 °C) to 66 wt% (600 °C) similarly to pyrolysis. From 700 °C, the carbon content in char decreases to 40 wt% (at 900 °C) due to gasification reactions. The char represents at 900 °C, 14 wt% of the initial carbon present in the digestate. Therefore, most of the carbon from char is transferred to gas. At 900 °C, the char presents an ash content of 53 wt%. The N/C atomic ratio of chars from pyrolysis and gasification is presented in supplementary material. The N/C ratio of the char from steam gasification is always higher for all reactor temperatures than that from pyrolysis. Nevertheless, in terms of N yields (N mass in char/N mass in digestate), steam promotes the conversion of N atoms from char to volatiles compared to pyrolysis from 800 °C (see Figure S3).

It was not possible to analyse solid carbon from combustion experiments due to their low mass and high dilution in the sand bed.

Van Krevelen diagram (Fig. 4) highlights the importance of dehydration reaction [40] on the evolution of char composition at different pyrolysis temperatures notably at 400 °C and 500 °C. Furthermore, at higher temperatures, the contribution of decarboxylation becomes more significant (in combination to dehydration). These results are in agreement with the literature [41,42]. Indeed, the H/C ratio of chars mainly depends on the final temperature in the pyrolysis reactor. It reflects the elemental atomic structure of the biochar (such as the size of the aromatic clusters) [42].

For steam gasification chars, the evolution from 400 °C to 600 °C is similar as for pyrolysis chars. The dehydration reaction is the main

Table 1
Elemental analysis of the chars.

Process type	Temperature (°C)	N [wt% db]	C [wt% db]	H [wt% db]	S [wt% db]
Pyrolysis	400	2.92 ± 0.09	58.36 ± 1.6	3.13 ± 0.08	0.85 ± 0.02
	500	2.42 ± 0.12	62.86 ± 0.67	2.34 ± 0.02	0.77 ± 0.11
	600	2.49 ± 0.03	65.25 ± 0.71	1.77 ± 0.1	0.94 ± 0.07
	700	2.19 ± 0.24	66.19 ± 0.36	1.05 ± 0.07	1.53 ± 0.28
	800	1.63 ± 0.05	66.57 ± 1.19	0.78 ± 0.41	1.51 ± 0.07
	900	1.30 ± 0.7	67.57 ± 1.14	0.65 ± 0.15	1.54 ± 0.03
Steam gasification	400	3.68 ± 0.21	59.11 ± 0.76	3.64 ± 0.04	0.94 ± 0.02
	500	3.42 ± 0.28	63.29 ± 0.08	2.71 ± 0.16	0.93 ± 0.06
	600	3.29 ± 0.23	66.12 ± 0.48	2.26 ± 0.06	0.91 ± 0.09
	700	2.32 ± 0.13	63.93 ± 1.33	1.59 ± 0.03	0.78 ± 0.07
	800	1.72 ± 0.04	53.95 ± 1.13	0.98 ± 0.02	0.84 ± 0.02
	900	1.85 ± 0.1	39.67 ± 0.51	0.59 ± 0.15	1.08 ± 0.04

evolution line [40] in the Van Krevelen diagram. From 700 °C, the O/C ratio is higher for gasification chars compared to the pyrolysis chars produced at the same temperature. The O/C ratio of steam chars are higher at 700 °C and 800 °C than the ones of pyrolysis chars because the formation of oxygen functional groups occurs more rapidly than their decomposition and release as CO and CO_2 [43]. Steam gasification chars present higher H/C ratio compared to pyrolysis chars (Fig. 4). It has been shown that contacting chars with steam produces high concentrations of reactive intermediates (especially H) that penetrate into the char matrix and that react with the carbonaceous moieties impacting aromatic clusters' size and surface functional groups [43,44].

Fig. 5 presents the principal component analysis (PCA) of the FTIR analysis of chars. It enables to differentiate the significant differences on the surface composition of chars (based on their FTIR analysis).

The loadings for PC-1 and PC-2 of PCA analysis are presented in supplementary material (Figure S4). FTIR analysis confirms the results obtained by elemental analysis: the chars produced at 400–600 °C are not significantly different between gasification and pyrolysis. They are grouped in Fig. 5. It confirms the poor chemical effect of steam on chars under these conditions (until 600 °C). Then the chars produced by pyrolysis or gasification are clearly differentiated above 700;°C (Fig. 5). This finding indicates that steam presents a significant impact on the surface chemistry of chars leading to the formation of surface functional groups [45,46] (mainly C-O moieties at around 1000 cm^{-1}, see Figure S4).

The characterization of chars has been completed by the analysis of their porous structure (Table 2).

The N_2 sorption isotherms are presented in supplementary material (Figure S5). Table 2 presents a slight increase in the surface area during pyrolysis up to 900 °C (68 m^2/g). Indeed, the increase in pyrolysis temperature can lead to the production of higher surface area chars [38]. Steam considerably increases the surface areas and pores volumes of the chars (compared to pyrolysis) from 700 °C by physical activation [46,47]. At 900 °C, steam gasification results in a reduction in the specific surface area because at higher char conversion the micropores begin to coalesce into larger pores (macropores and mesopores), which decreases the surface area [48,49].

3.3. Gas composition

The gas mass yields are presented in Fig. 6. Molar compositions of gases are presented in supplementary material.

For pyrolysis, CO_2 is the major gas at low temperatures formed by primary decarboxylation reactions [39,50,51]. This result is in agreement with the literature on digestates pyrolysis [9,10,22–24]. Then, secondary reactions (conversion of tar) promote the formation of the other gases as a function of the freeboard temperature [25,36]. Hydrocarbons (CH_4, C_2) are not converted by secondary reactions under the conditions of this study (gas residence time of 1.2 s in the freeboard), which is in agreement with previous work [36,52,53].

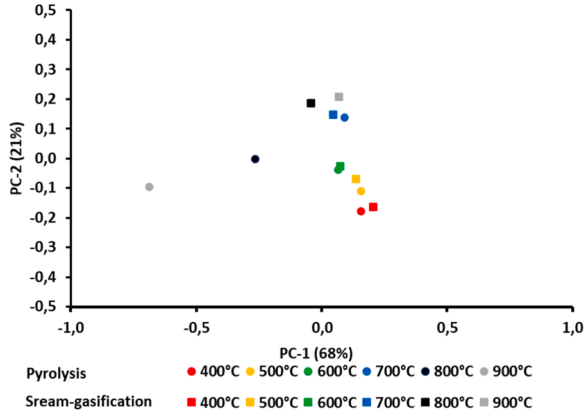

Fig. 5. PCA of FTIR spectra of chars from pyrolysis and steam gasification.

Table 2
Specific surface area and pore volume of chars from pyrolysis and steam-gasification.

Process type	Temperature (°C)	A_{BET} (m^2/g)	$V_{0.95}$ (cm^3/g)[a]
Pyrolysis	600	6	0.01
	700	5	0.01
	800	16	0.01
	900	68	0.04
Steam gasification	600	11	0.01
	700	337	0.16
	800	461	0.26
	900	374	0.25

[a] $V_{0.95}$ (cm^3/g) corresponds to the adsorbed volume at a relative pressure of 0.95

For steam gasification, the mass yields in gas are presented in Fig. 6b). Compared to pyrolysis, the mass yields of all gases are similar until 500 °C. Then, above 600 °C, an important increase in H_2 formation is observed (mass yields of 3.6 wt% at 900 °C with H_2O vs. 1.1 wt% for pyrolysis at 900 °C). Methane mass yields are similar for steam gasification and pyrolysis. It is not impacted by the presence of steam confirming the poor chemical effect of H_2O for methane gas-phase reforming at a gas-phase residence time of 1.2 s [53]. CO is competitively formed by char gasification and converted by water gas-shift leading to an important increase in CO_2 and H_2 mass yields. At 900 °C, CO_2 and CO present mass yields of 41 wt% and 26 wt%, respectively, for steam gasification (vs. 15 wt% and 22.5 wt%, respectively, for pyrolysis). The experimental gas composition obtained for steam gasification is compared to the thermodynamic equilibrium in supporting material. The thermodynamic equilibrium is not achieved under the conditions of this study (gas-phase residence time of 1.2 s). This result is in agreement with previous works [54–56].

For partial combustion, the mass yield in gas is presented in Fig. 6c. CO_2 is the major products even at 400 °C. H_2 formed during pyrolysis is further oxidized by air at all temperatures. CH_4 and C_2H_4 are clearly converted from 800°C by oxidation in the freeboard, but their conversion is not complete due to kinetic limitations (short gas-phase residence time). The CO/CO_2 ratio increases from 0.13 ($molCO/molCO_2$) at 400 °C to 0.37 at 900;°C. This trend is in agreement with previous work on chars combustion in fluidized beds [57–59]. CO is competitively formed by primary pyrolysis, oxidation of pyrolysis products (gas, tar and char) and converted to CO_2 by oxidation.

The global conversion of carbon from digestates to the gas is presented in Table 3.

For pyrolysis and steam gasification, the conversion of carbon from digestates to the gas (mainly to CO_2) is similar at 400 °C and 500 °C. For steam gasification, the total carbon content of gas represents 6 wt% of the initial carbon (present in the digestate) at 400;°C and 59 wt% at 900 °C (instead of 43 wt% for pyrolysis). Therefore, at 900 °C, 16 wt% of the carbon is transferred from the char to the gas stream by the steam gasification reactions. Concerning combustion, 50 wt% of carbon is already transferred in the gas at 400 °C (mainly as CO_2) and 84 % at 900 °C. Oxidation reactions are probably limited by kinetic or hydrodynamic factors considering the partial consumption of O_2 (presented in supporting material).

The results of quantification for NH_3 (by spectrophotometry) and HCN (by FTIR) are presented in Fig. 7.

The formation of N-species and notably the NH_3/HCN ratio mainly depends on the composition in amino-acids of the biomasses [60]. It is known that sludges produce NH_3 as a major N-product during fast pyrolysis between 400 and 700 °C [61]. NH_3 is the major nitrogenous gas for all our conditions (Fig. 7) in agreement with Cao et al. [61]. NH_3 is formed by the pyrolysis of amine groups [62] at temperatures lower than 500 °C under our conditions. Steam slightly promotes NH_3

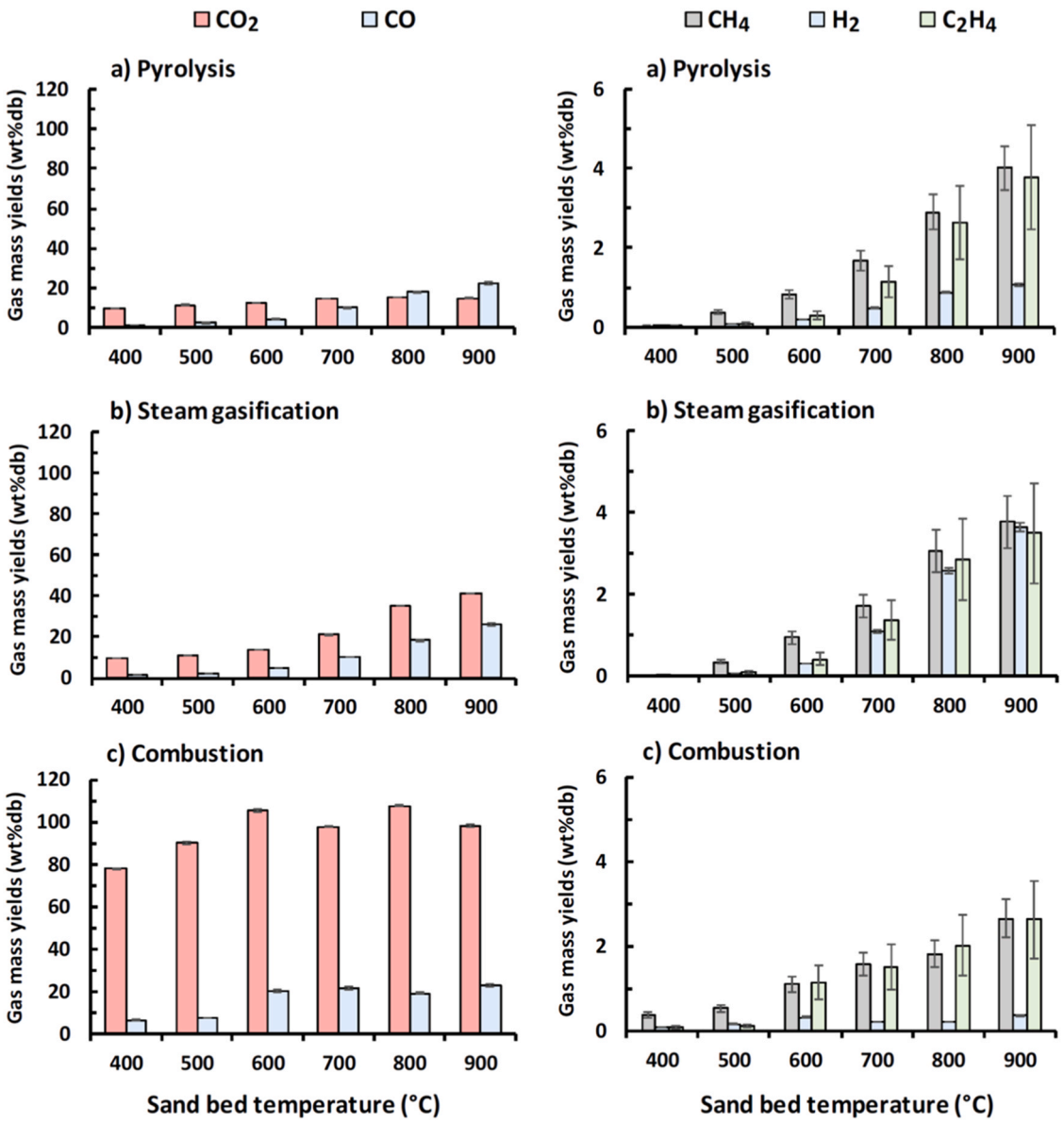

Fig. 6. Mass yields (wt% db based on anhydrous digestate mass) of gases for a) pyrolysis, b) steam gasification, c) partial combustion at different fluidized sand temperatures.

Table 3
Conversion of carbon from digestates to gas (wt%, g C in gas/g C in digestate).

Temperature of fluidized sand	400°C	500°C	600°C	700°C	800°C	900°C
Pyrolysis	7	10	13	23	35	43
Steam-gasification	6	9	15	28	48	59
Combustion	50	58	80	78	84	84

formation in agreement with a previous work explaining this increase in NH_3 by a potential hydrogenation of char-N moieties by H radicals [63]. NH_3 seems only slightly converted at 900 °C. We did not notice an effect of oxygen under our conditions on NH_3 conversion. This high stability of NH_3 (even at 900 °C) is consistent with previous work [33,64]. NOx were not detected by FTIR analysis of the gas. This result is in agreement with previous work showing a very low formation of NO from NH_3 conversion even at 900 °C under oxidation conditions [64].

At 900 °C, the yield in HCN is similar for pyrolysis, gasification and combustion. It is interesting to note the increase in HCN from 700 °C and an important increase at 900 °C. Cao et al.[61] also found an increase in HCN from 500 to 700 °C during the pyrolysis of sludges (but not on the same type of digestates as this present study) in a drop tube reactor. Kwapinska et al. [33] presented a comprehensive analysis of N-species from the pyrolysis of dairy sludges and these authors also showed an increase in HCN yields up to 900 °C. The mechanisms of nitrogen migration during sludges thermochemical conversion were extensively reviewed [65–68]. The formation of HCN may be explained by the conversion of amide [60,61,69], pyrrole and pyridine groups [62].

3.4. Characterization of the liquids

The liquids were analyzed by GC/MS-FID. A detailed characterization of about 30 detected peaks is presented in supporting information. But these 30 species still account for a minor mass fraction of the bio-oil (less than 2 wt% of the digestate mass). Fig. 8 shows the evolution of the major type of species quantified by GC/MS as a function of reactor temperatures.

Fig. 8 highlights that the major compounds at 400 °C and 500 °C are

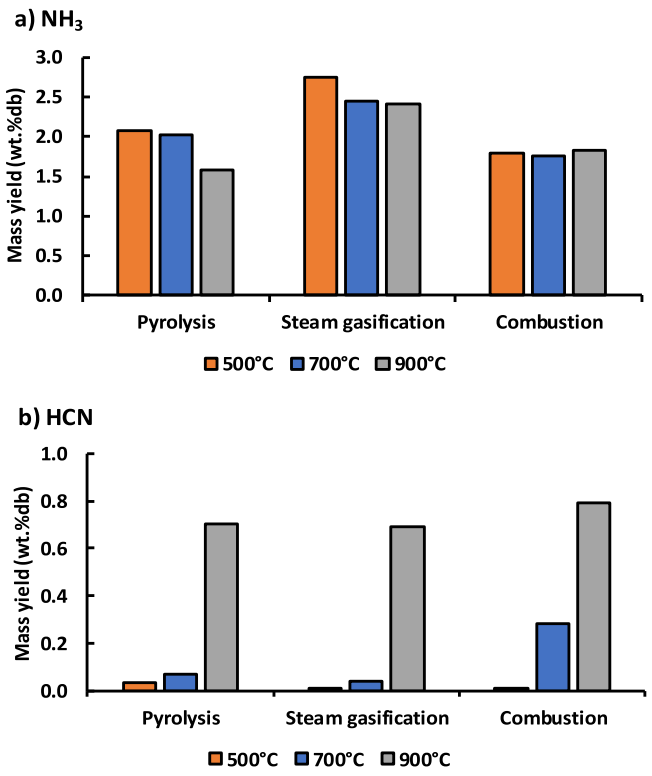

Fig. 7. NH_3 and HCN quantification (wt%db, based on anhydrous digestate mass).

acids (acetic acid), methoxy-phenols (like 2-methoxy-4-vinylphenol as a main species) and furans (mainly as benzofuran, 2,3-dihydro-) for the three fluidizing gas. This result is in agreement with previous work on the pyrolysis of digestates [6,20]. Steam promotes the formation of phenols and furans compared to pyrolysis. The yield in aromatic hydrocarbons increase from 800 °C for the three processes.

For pyrolysis and steam gasification, methoxy-phenols are converted from 600 °C and furans from 800 °C. Methoxy-phenols are primary products[70] and they are converted from 600 °C to phenol, a secondary product[70]. Phenol is, mainly, formed between 600 °C and 800 °C and competitively converted (notably at 900 °C) to aromatic hydrocarbons, in agreement with previous work[52,70,71]. Concerning gasification, Fig. 8 confirms that steam does not promote (compared to N_2) the secondary gas-phase conversion (in our freeboard) of phenol or aromatic hydrocarbons [72]. The GC/MS analysis (Fig. 8c) clearly shows the important effect of air (O_2) on the secondary reactions occurring in the free-board of the fluidized bed (for a gas-phase residence time of 1.2 s). From 600 °C, air seems to promote the conversion of acids, methoxyl-phenols and furans. The conversion of aromatic hydrocarbons is promoted by air (compared to steam or N_2) at 900 °C.

GC/MS identifies a small fraction of organic liquid products (only less than 2 wt% of the digestate mass). For this reason, the analysis by high resolution mass spectrometry (FT-ICR MS) was performed in order to complete the characterization of the liquids.

Molecular compositions of all bio-oils obtained by FT-ICR MS measurement are given in Fig. 9 and S8.

It is noteworthy to highlight the good repeatability of the conversion processes. Indeed, the replicate analysis of two different bio-oils produced by two different pyrolysis experiments (pyrolysis and steam gasification) gave similar DBE, O/C, and H/C values (Table 4), as well as close molecular composition descriptions (Fig. 9).

Between 9000 and 3000 different molecular formulae were found for each sample, demonstrating their high molecular complexity. CHNyOx molecular series mostly contributes to the sample description, followed

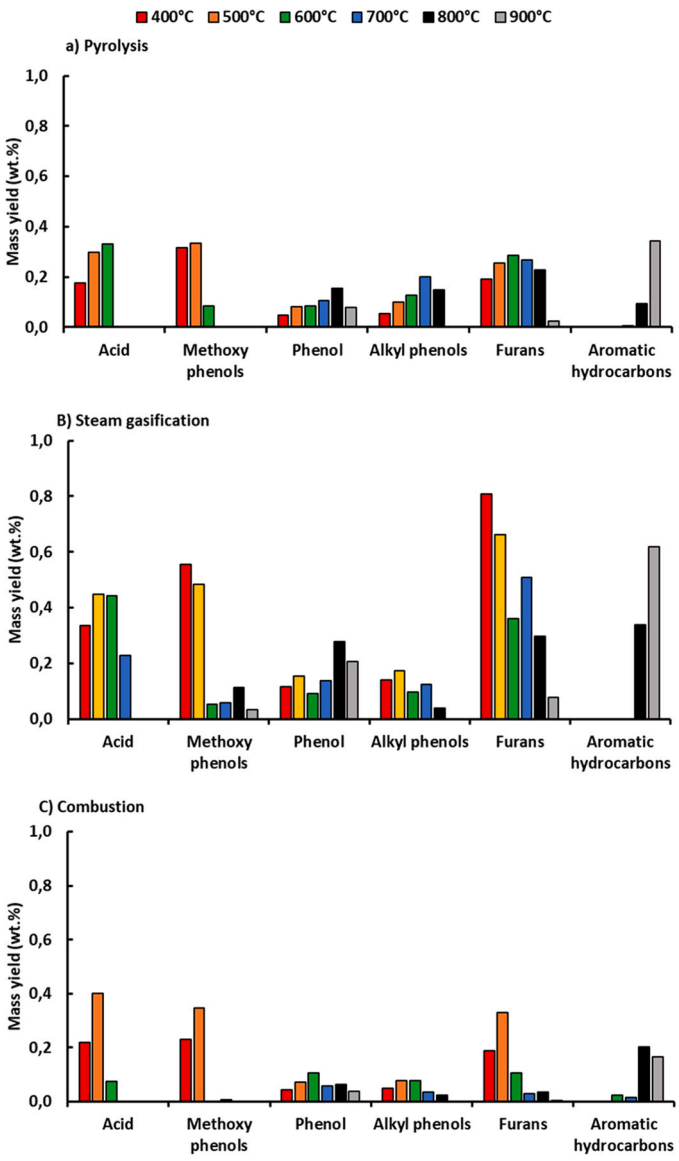

Fig. 8. Evolution of mass yields (wt%db, based on anhydrous digestate mass) of main species at different fluidized sand temperatures: a) pyrolysis, b) steam gasification, c) combustion.

by the CHOx class. The high contribution of the nitrogen-containing compounds was also observed by ESI (+) FT-ICR MS analyses of bio-oils from waste [73,74].

Regardless of the thermochemical conversion process, fewer compounds were detected upon increasing temperature. This decrease in the overall number of compounds is specifically to the benefit of CHNx compounds, whose number increases. This is consistent with FTIR analyses of the gas that measured an increase in the amount of HCN with the conversion temperature due to the secondary conversion of CHNyOx species. Secondary reactions are promoted at higher reactor temperature, which also results to less oxygen-containing and lower-mass compounds [75,76]. Oxygen content decreasing with increasing temperatures was observed with the decrease of the O/C value. It is well known that secondary gas-phase reactions in the freeboard promote conversion of oxygenated species and the formation of aromatic hydrocarbons [52,70,71]. This is consistent with the GC/MS analysis showing the increase in aromatic hydrocarbons species with the temperature. This fact is also evidenced in this study with higher Double Bound Equivalent (DBE – see supplementary materials) value of bio-oil components at higher reactor temperatures, regardless the atmosphere

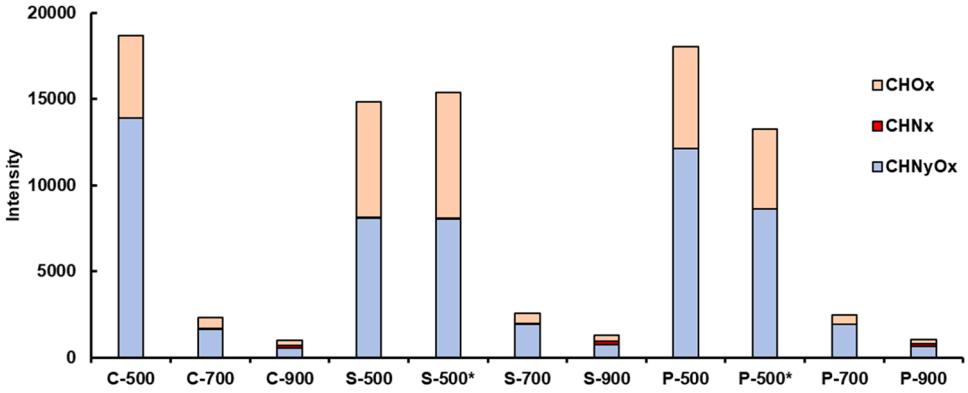

Fig. 9. Heteroatom class distributions,with the sum of the normalized intensities, achieved by ESI (+) FT-ICR MS analysis of bio-oil samples from combustion (C), steam gasification (S), and pyrolysis (P) at different temperatures. *Refers to pyrolysis and steam gasification replicate samples.

Table 4
Weighted averages of DBE, O/C, and H/C calculated from the assignments obtained by ESI (+) FT-ICR MS analysis of bio-oil samples from combustion (C), steam gasification (V), and pyrolysis (P) at different temperatures.

Samples	DBE	O/C	H/C
P−500 °C	7.37	0.35	1.41
P−500 °C[a]	7.30	0.36	1.42
P−700 °C	8.36	0.25	1.37
P−900 °C	9.77	0.17	1.24
S−500 °C	7.21	0.36	1.41
S−500 °C[a]	7.01	0.36	1.42
S−700 °C	8.55	0.24	1.32
S−900 °C	9.86	0.13	1.26
C−500 °C	7.36	0.34	1.40
C−700 °C	9.84	0.19	1.19
C−900 °C	9.79	0.14	1.27

[a] Refers to pyrolysis and steam gasification replicate samples.

conditions (Table 4). Thus, bio-oil compounds are less polar, which makes them less or not ionizable by ESI [77]. Therefore, it also explains the decreasing number of detected compounds with increasing temperatures.

The repeatability of the conversion processes and FT-ICR MS analysis, as well as the temperature influence on the bio-oil composition, were also evidenced on the Principal Component Analysis (PCA) score plots (Fig. 10).

Indeed, samples are ordered within the first component according to the temperature parameter. The samples obtained at 500 °C present higher variability in their composition than those obtained at 700 and 900 °C. This result is in agreement with a previous study conducted on liquids composition as a function of reactor temperatures [78]. This is mainly due to the number of molecular contributions describing these samples, but the research profiles allowed to extract the molecular assignments specific to each conversion temperature (Figure S9), which emphasized the previous observations. With temperature increase, contribution of the CHOx class decreases, and O/C values too, while the CHNx one increases, as well as the DBE value.

Within the second component (in Fig. 10), bio-oil compositions differ according to the atmospheric conditions (air, water, N_2), especially for the samples obtained at 500 °C. Indeed, at this temperature, it is clearly observed that bio-oils produced at one atmospheric condition clustered on the PCA plot. However, over the different temperatures, the bio-oils from combustion have a different behavior compared to those obtained after pyrolysis and steam gasification based on the distance between the plots. This result is in agreement with the effect of O_2 evidenced by GC/MS. To better understand what is responsible for these variations, research profiles were done for each of the pyrolysis, combustion, and

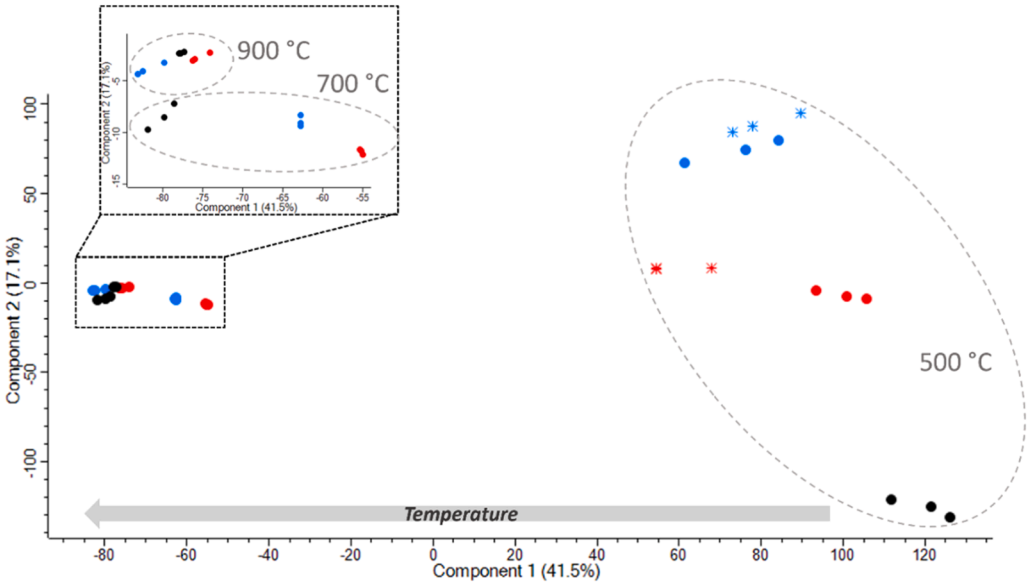

Fig. 10. PCA score plot of all assigned *m/z* features obtained by ESI (+) FT-ICR MS of bio-oil samples from combustion (black), steam gasification (blue), and pyrolysis (red) at different temperatures.

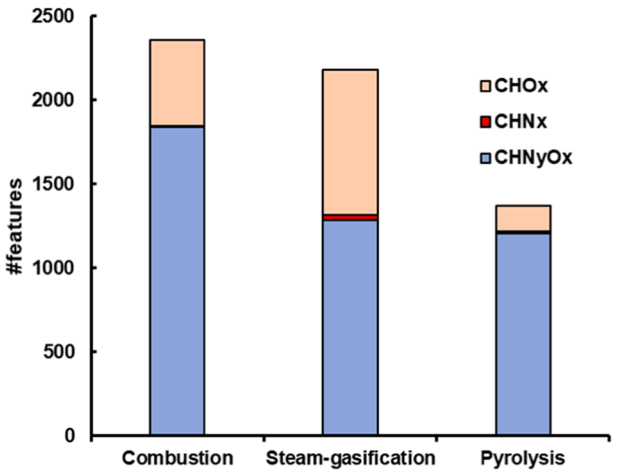

Fig. 11. Heteroatom class distributions of the molecular assignments, obtained by ESI (+) FT-ICR MS, specific to each atmospheric condition at 500°C.

steam gasification samples at 500 °C as they present the highest compositional differences. This enabled to extract and to plot the specific compounds (Fig. 11).

Steam gasification sample exhibits more CHOx and CHNx compounds, but overall, CHNyOx series is predominant in the sample descriptions. In order to unravel a better insight into the bio-oil compositions and to highlight molecular differences within the samples, N-compounds were plotted on van Krevelen diagrams (Fig. 12).

Fig. 12 shows that bio-oil from combustion is characterized by more oxygenated N-compounds, with higher O/C values, which are not observed on the two other van Krevelen diagrams. Air presents an important effect on the molecular species even at 500 °C and notably at 700 °C (Fig. 10), with the promotion of CHNO species formation (Fig. 9) even at 500 °C.

Steam gasification and pyrolysis bio-oils are more similar with nitrogen-containing compounds having O/C < 0.6. FT-ICR MS confirms aforementioned poor chemical effect of H_2O based on DBE, O/C, and H/C (Table 4). Steam seems to promote the CHOx classes at 500 °C compared to pyrolysis (Fig. 9). The PCA confirms that steam presents fewer chemical effects than air at 500°C and 700°C.

These results confirm that gas atmosphere has a significant impact on the bio-oil composition, particularly at 500 °C. At higher temperatures, the differences between atmosphere composition is lower, this means that the composition of the liquids is more controlled by temperatures than by atmosphere (at 900 °C), due to the predominance of secondary reactions in agreement with previous work.[70,71]

4. Conclusion

To the best of our knowledge, we present the first study on the pyrolysis, gasification and combustion of digestates in a fluidized bed. The complete set of analyses enables to unravel the effect of steam and air on the products mass yields and on their composition.

Our main findings are the followings:

1) Steam does not present a significant effect on char elemental composition between 400 °C and 600 °C. However, from 700 °C, the carbon content in char decreases due to gasification reaction down to 39 wt% C at 900 °C. Steam promotes the conversion of N atoms into volatiles compared to pyrolysis from 800 °C.
2) Air leads to an important oxidation of char and volatiles even at 400 °C.
3) Methane mass yield is similar for both steam gasification and pyrolysis even at high temperatures. It is not impacted by the presence of H_2O confirming the low reactivity of H_2O on methane gas-phase reforming with a gas-phase residence time of 1.2 s. Furthermore, air clearly promotes the conversion of all hydrocarbons from 800 °C.
4) CO yield becomes higher for steam gasification than for pyrolysis from 800 °C, highlighting the importance of char gasification at 800°C and 900 °C. CO is competitively formed by char gasification and converted by water gas-shift leading to an important increase in CO_2 and H_2 yields.
5) NH_3 is the major N-gas species for all conditions. It is not significantly converted under our conditions. HCN is an important product increasing from 700 °C and notably at 900 °C.
6) Both GC/MS and FT-ICR MS reveal that steam presents a poor chemical effect on the organic molecules present in the liquids. Air exhibits an important reactivity even from 400 °C. PCA analysis conducted on the FT-ICR MS analysis clearly differentiate the gas atmosphere (and O_2 notably at 500 °C). At 900 °C, all liquid samples are very similar highlighting the more significant effect of temperature than the reactive gas at 900 °C. For all conditions, the temperature increases DBE and reduces the oxygenated species. The class CHN (in liquid) is mainly observed at 900 °C which is consistent with the increase in HCN molecule as analyzed in the gas by FTIR.

The syngas (promoted by steam gasification) should be further upgraded to produce purified H_2, liquid fuels and/or electricity (by combustion in a gas engine). The bio-oils promoted at 500–600 °C by fast pyrolysis in the fluidized bed also require an up-grading process (deoxygenation, denitrogenation) to produce chemicals or liquid fuels. Char can be further activated to produce high-value activated carbons with tailored porous structure and surface functional groups.

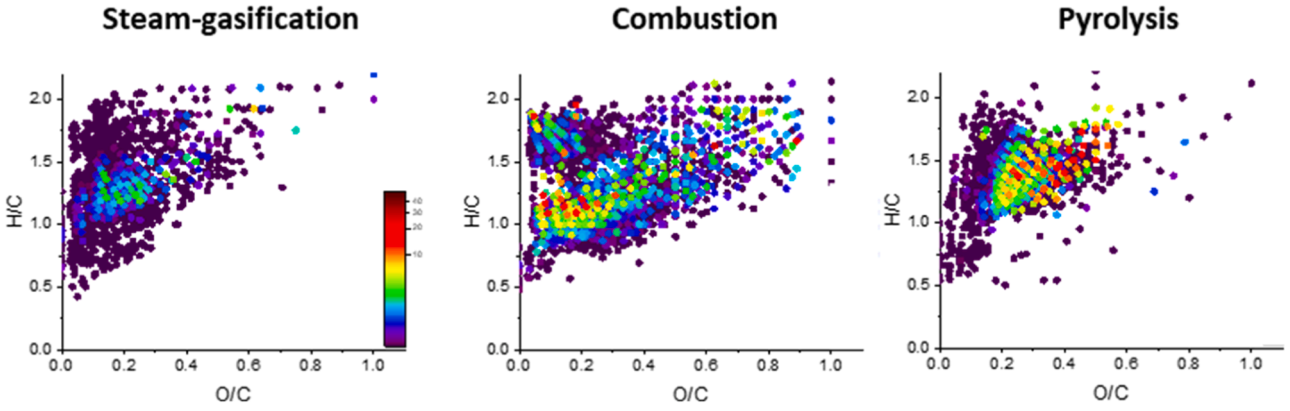

Fig. 12. Van Krevelen diagrams of the CHNx and CHNyOx compounds obtained by ESI (+) FT-ICR MS, specific to each atmospheric condition at 500 °C. The color scale represents the relative intensity of the assigned *m/z* signals.

Supporting information

The supporting information file presents: (1) details on analysis and preparation of digestates; (2) effect of digestate pretreatment on pyrolysis mass yields; (3) O_2 consumed and stoichiometry for combustion; (4) composition (C, N, H), FTIR and N_2 sorption analysis of chars; (5) gas composition; (6) detailed characterization of liquids by GC/MS and FTICRMS.

CRediT authorship contribution statement

Mohamed H. Aissaoui: Writing – original draft, Visualization, Validation, Methodology, Investigation, Formal analysis, Data curation. **Anthony Dufour:** Writing – review & editing, Writing – original draft, Visualization, Validation, Supervision, Resources, Project administration, Methodology, Investigation, Funding acquisition, Formal analysis, Data curation, Conceptualization. **Marie-Noelle Pons:** Writing – review & editing, Investigation, Formal analysis, Data curation, Conceptualization. **Jasmine Hertzog:** Writing – review & editing, Software, Formal analysis, Data curation. **Paola Gauthier-Maradei:** Writing – review & editing, Validation, Supervision, Project administration, Methodology, Funding acquisition, Conceptualization. **Yann Le Brech:** Visualization, Validation, Methodology, Formal analysis, Data curation, Conceptualization. **Vincent Carre:** Writing – review & editing, Project administration, Methodology, Data curation. **Cecilia Sambusiti:** Writing – review & editing, Validation, Supervision, Conceptualization.

Declaration of Competing Interest

The authors declare the following financial interests/personal relationships which may be considered as potential competing interests: Anthony DUFOUR group reports financial support was provided by Total Energies.

Acknowledgements

This work was partially supported by the MassLor research infrastructure at the University of Lorraine, for FT-ICR MS analyses.

Appendix A. Supporting information

Supplementary data associated with this article can be found in the online version at doi:10.1016/j.jaap.2024.106928.

Data availability

Data will be made available on request.

References

[1] M. Pecchi, M. Baratieri, Coupling anaerobic digestion with gasification, pyrolysis or hydrothermal carbonization: a review, Renew. Sustain. Energy Rev. 105 (2019) 462–475, https://doi.org/10.1016/j.rser.2019.02.003.
[2] F. Monlau, C. Sambusiti, E. Ficara, A. Aboulkas, A. Barakat, H. Carrère, New opportunities for agricultural digestate valorization: current situation and perspectives, Energy Environ. Sci. 8 (2015) 2600–2621, https://doi.org/10.1039/c5ee01633a.
[3] C.A. Sevillano, A.A. Pesantes, E. Peña Carpio, E.J. Martínez, X. Gómez, Anaerobic digestion for producing renewable energy-the evolution of this technology in a new uncertain scenario, Entropy 23 (2021) 1–23, https://doi.org/10.3390/e23020145.
[4] W. Wang, D.J. Lee, Valorization of anaerobic digestion digestate: a prospect review, Bioresour. Technol. 323 (2021) 124626, https://doi.org/10.1016/j.biortech.2020.124626.
[5] D. Maria, M. Fongen, F. Bente, Greenhouse gas emissions from digestate in soil, Int. J. Recycl. Org. Waste Agric. (2020) 1–7, https://doi.org/10.30486/IJROWA.2020.1885341.1005.
[6] J.V. Karaeva, S.S. Timofeeva, V.N. Bashkirov, K.S. Bulygina, Thermochemical processing of digestate from biogas plant for recycling dairy manure and biomass, Biomass Convers. Bioref. (2021), https://doi.org/10.1007/s13399-020-01138-6.
[7] J.A. Okolie, E.I. Epelle, M.E. Tabat, U. Orivri, A.N. Amenaghawon, P.U. Okoye, et al., Waste biomass valorization for the production of biofuels and value-added products: A comprehensive review of thermochemical, biological and integrated processes, Process Saf. Environ. Prot. 159 (2022) 323–344, https://doi.org/10.1016/j.psep.2021.12.049.
[8] V.S. Sikarwar, M. Pohořelý, E. Meers, S. Skoblia, J. Moško, M. Jeremiáš, Potential of coupling anaerobic digestion with thermochemical technologies for waste valorization, Fuel 294 (2021), https://doi.org/10.1016/j.fuel.2021.120533.
[9] S. Tayibi, F. Monlau, F. Marias, N. Thevenin, R. Jimenez, A. Oukarroum, et al., Industrial symbiosis of anaerobic digestion and pyrolysis: performances and agricultural interest of coupling biochar and liquid digestate, Sci. Total Environ. 793 (2021) 148461, https://doi.org/10.1016/j.scitotenv.2021.148461.
[10] J. Neumann, J. Meyer, M. Ouadi, A. Apfelbacher, S. Binder, A. Hornung, The conversion of anaerobic digestion waste into biofuels via a novel thermo-catalytic reforming process, Waste Manag. 47 (2016) 141–148, https://doi.org/10.1016/j.wasman.2015.07.001.
[11] F. Monlau, C. Sambusiti, N. Antoniou, A. Barakat, A. Zabaniotou, A new concept for enhancing energy recovery from agricultural residues by coupling anaerobic digestion and pyrolysis process, Appl. Energy 148 (2015) 32–38, https://doi.org/10.1016/j.apenergy.2015.03.024.
[12] A. Dieguez-Alonso, A. Funke, A. Anca-Couce, A.G. Rombolà, G. Ojeda, J. Bachmann, et al., Towards biochar and hydrochar engineering—influence of process conditions on surface physical and chemical properties, thermal stability, nutrient availability, toxicity and wettability, Energies 11 (2018) 496, https://doi.org/10.3390/en11030496.
[13] C.A. Takaya, L.A. Fletcher, S. Singh, K.U. Anyikude, A.B. Ross, Phosphate and ammonium sorption capacity of biochar and hydrochar from different wastes, Chemosphere 145 (2016) 518–527, https://doi.org/10.1016/j.chemosphere.2015.11.052.
[14] D. Rodríguez Alberto, A.C. Tyler, T.A. Trabold, Phosphate adsorption using biochar derived from solid digestate, Bioresour. Technol. Rep. 16 (2021) 100864, https://doi.org/10.1016/j.biteb.2021.100864.
[15] I. Piccoli, A. Torreggiani, C. Pituello, A. Pisi, F. Morari, O. Francioso, Automated image analysis and hyperspectral imagery with enhanced dark field microscopy applied to biochars produced at different temperatures, Waste Manag. 105 (2020) 457–466, https://doi.org/10.1016/j.wasman.2020.02.037.
[16] W. Peng, H. Zhang, F. Lü, L. Shao, P. He, Char derived from food waste based solid digestate for phosphate adsorption, J. Clean. Prod. 297 (2021) 126687, https://doi.org/10.1016/j.jclepro.2021.126687.
[17] Y. Qiao, S. Zhang, C. Quan, N. Gao, C. Johnston, C. Wu, One-pot synthesis of digestate-derived biochar for carbon dioxide capture, Fuel 279 (2020) 118525, https://doi.org/10.1016/j.fuel.2020.118525.
[18] E. Miliotti, D. Casini, L. Rosi, G. Lotti, A.M. Rizzo, D. Chiaramonti, Lab-scale pyrolysis and hydrothermal carbonization of biomass digestate: Characterization of solid products and compliance with biochar standards, Biomass Bioenergy 139 (2020) 105593, https://doi.org/10.1016/j.biombioe.2020.105593.
[19] A. Funke, F. Reebs, A. Kruse, Experimental comparison of hydrothermal and vapothermal carbonization, Fuel Process. Technol. 115 (2013) 261–269, https://doi.org/10.1016/j.fuproc.2013.04.020.
[20] Y. Wei, J. Hong, W. Ji, Thermal characterization and pyrolysis of digestate for phenol production, Fuel 232 (2018) 141–146, https://doi.org/10.1016/j.fuel.2018.05.134.
[21] B. Garcia, O. Alves, B. Rijo, G. Lourinho, C. Nobre, Biochar: production, applications, and market prospects in Portugal, Environments 9 (2022) 95, https://doi.org/10.3390/environments9080095.
[22] J. Zhao, Z. Wang, J. Li, B. Yan, G. Chen, Pyrolysis of food waste and food waste solid digestate: a comparative investigation, Bioresour. Technol. 354 (2022) 127191, https://doi.org/10.1016/j.biortech.2022.127191.
[23] F. Monlau, C. Sambusiti, N. Antoniou, A. Barakat, A. Zabaniotou, A new concept for enhancing energy recovery from agricultural residues by coupling anaerobic digestion and pyrolysis process, Appl. Energy 148 (2015) 32–38, https://doi.org/10.1016/j.apenergy.2015.03.024.
[24] S. Tayibi, F. Monlau, F. Marias, G. Cazaudehore, N.-E. Fayoud, A. Oukarroum, et al., Coupling anaerobic digestion and pyrolysis processes for maximizing energy recovery and soil preservation according to the circular economy concept, J. Environ. Manag. 279 (2021) 111632, https://doi.org/10.1016/j.jenvman.2020.111632.
[25] M.J. Antal, Effects of reactor severity on the gas-phase pyrolysis of cellulose- and kraft lignin-derived volatile matter, Ind. Eng. Chem. Prod. Res. Dev. 22 (1983) 366–375, https://doi.org/10.1021/i300010a039.
[26] G. Chen, X. Guo, Z. Cheng, B. Yan, Z. Dan, W. Ma, Air gasification of biogas-derived digestate in a downdraft fixed bed gasifier, Waste Manag. 69 (2017) 162–169, https://doi.org/10.1016/j.wasman.2017.08.001.
[27] M. Baláš, P. Milčák, P. Elbl, M. Lisý, J. Lachman, P. Kracík, Gasification of fermentation residue in a fluidised-bed gasifier, Energy 245 (2022), https://doi.org/10.1016/j.energy.2022.123211.
[28] M. Kratzeisen, N. Starcevic, M. Martinov, C. Maurer, J. Müller, Applicability of biogas digestate as solid fuel, Fuel 89 (2010) 2544–2548, https://doi.org/10.1016/j.fuel.2010.02.008.
[29] L.Y. Jia, M. Raad, S. Hamieh, J. Toufaily, T. Hamieh, M.M. Bettahar, et al., Catalytic fast pyrolysis of biomass: superior selectivity of hierarchical zeolites to aromatics, Green Chem. 19 (2017) 5442–5459, https://doi.org/10.1039/C7GC02309J.
[30] X. Liu, G. Xu, S. Gao, Micro fluidized beds: wall effect and operability, Chem. Eng. J. 137 (2008) 302–307, https://doi.org/10.1016/j.cej.2007.04.035.
[31] R. Olcese, V. Carré, F. Aubriet, A. Dufour, Selectivity of bio-oils catalytic hydrotreatment assessed by petroleomic and GC*GC/MS-FID analysis, Energy Fuels 27 (2013) 2135–2145, https://doi.org/10.1021/ef302145g.

[32] J. Hertzog, V. Carré, Y. Le Brech, A. Dufour, F. Aubriet, Toward controlled ionization conditions for ESI-FT-ICR-MS analysis of bio-oils from lignocellulosic material, Energy Fuels 30 (2016) 5729–5739, https://doi.org/10.1021/acs.energyfuels.6b00655.
[33] M. Kwapinska, P. Sommersacher, N. Kienzl, S. Retschitzegger, J. Lagler, A. Horvat, et al., Release of N-containing compounds during pyrolysis of milk/dairy processing sludge – experimental results and comparison of measurement techniques, J. Anal. Appl. Pyrolysis 178 (2024) 106391, https://doi.org/10.1016/j.jaap.2024.106391.
[34] M. Bechikhi, E. Masson, O. Herbinet, A. Dufour, Mapping of tobacco conversion characteristics in electrically heated systems: effect of air and temperatures on the onset of combustion and formation of volatile species, J. Anal. Appl. Pyrolysis 184 (2024) 106847, https://doi.org/10.1016/j.jaap.2024.106847.
[35] R. Venderbosch, W. Prins, Fast pyrolysis technology development, Biofuels, Bioprod. Bioref. 4 (2010) 178–208, https://doi.org/10.1002/bbb.205.
[36] D. Fuentes-Cano, A. Gómez-Barea, S. Nilsson, Generation and secondary conversion of volatiles during devolatilization of dried sewage sludge in a fluidized bed, Ind. Eng. Chem. Res 52 (2013) 1234–1243, https://doi.org/10.1021/ie302678u.
[37] J. Kramb, J. Konttinen, A. Gómez-Barea, A. Moilanen, K. Umeki, Modeling biomass char gasification kinetics for improving prediction of carbon conversion in a fluidized bed gasifier, Fuel 132 (2014) 107–115, https://doi.org/10.1016/j.fuel.2014.04.014.
[38] J.A. Ippolito, L. Cui, C. Kammann, N. Wrage-Mönnig, J.M. Estavillo, T. Fuertes-Mendizabal, et al., Feedstock choice, pyrolysis temperature and type influence biochar characteristics: a comprehensive meta-data analysis review, Biochar 2 (2020) 421–438, https://doi.org/10.1007/s42773-020-00067-x.
[39] D. Neves, H. Thunman, A. Matos, L. Tarelho, A. Gómez-Barea, Characterization and prediction of biomass pyrolysis products, Prog. Energy Combust. Sci. 37 (2011) 611–630, https://doi.org/10.1016/j.pecs.2011.01.001.
[40] D.C.P. Lozano, H.E. Jones, T.R. Reina, R. Volpe, M.P. Barrow, Unlocking the potential of biofuels via reaction pathways in van Krevelen diagrams, Green Chem. 23 (2021) 8949–8963, https://doi.org/10.1039/D1GC01796A.
[41] K. Weber, P. Quicker, Properties of biochar, Fuel 217 (2018) 240–261, https://doi.org/10.1016/j.fuel.2017.12.054.
[42] X. Xiao, Z. Chen, B. Chen, H/C atomic ratio as a smart linkage between pyrolytic temperatures, aromatic clusters and sorption properties of biochars derived from diverse precursory materials, Sci. Rep. 6 (2016) 22644, https://doi.org/10.1038/srep22644.
[43] Lahaye J., Ehrburger P. Fundamental issues in control of carbon gasification reactivity 1991.
[44] D.M. Keown, J.-I. Hayashi, C.-Z. Li, Drastic changes in biomass char structure and reactivity upon contact with steam, Fuel 87 (2008) 1127–1132, https://doi.org/10.1016/j.fuel.2007.05.057.
[45] R. Bardestani, S. Kaliaguine, Steam activation and mild air oxidation of vacuum pyrolysis biochar, Biomass Bioenergy 108 (2018) 101–112, https://doi.org/10.1016/j.biombioe.2017.10.011.
[46] J.L. Figueiredo, M.F.R. Pereira, M.M.A. Freitas, J.J.M. Órfão, Modification of the surface chemistry of activated carbons, Carbon 37 (1999) 1379–1389, https://doi.org/10.1016/S0008-6223(98)00333-9.
[47] N.L. Panwar, A. Pawar, Influence of activation conditions on the physicochemical properties of activated biochar: a review, Biomass Convers. Bioref. 12 (2022) 925–947, https://doi.org/10.1007/s13399-020-00870-3.
[48] G.Q. Lu, D.D. Do, Comparison of structural models for high-ash char gasification, Carbon 32 (1994) 247–263, https://doi.org/10.1016/0008-6223(94)90188-0.
[49] A. Zoulalian, R. Bounaceur, A. Dufour, Kinetic modelling of char gasification by accounting for the evolution of the reactive surface area, Chem. Eng. Sci. 138 (2015) 281–290, https://doi.org/10.1016/j.ces.2015.07.035.
[50] S. Wang, G. Dai, H. Yang, Z. Luo, Lignocellulosic biomass pyrolysis mechanism: a state-of-the-art review, Prog. Energy Combust. Sci. 62 (2017) 33–86, https://doi.org/10.1016/j.pecs.2017.05.004.
[51] J. He, V. Strezov, R. Kumar, H. Weldekidan, S. Jahan, B.H. Dastjerdi, et al., Pyrolysis of heavy metal contaminated Avicennia marina biomass from phytoremediation: characterisation of biomass and pyrolysis products, J. Clean. Prod. 234 (2019) 1235–1245, https://doi.org/10.1016/j.jclepro.2019.06.285.
[52] A. Dufour, E. Masson, P. Girods, Y. Rogaume, A. Zoulalian, Evolution of aromatic tar composition in relation to methane and ethylene from biomass pyrolysis-gasification, Energy Fuels 25 (9) (2011) 4182, https://doi.org/10.1021/ef200846g.
[53] A. Dufour, S. Valin, P. Castelli, S. Thiery, G. Boissonnet, A. Zoulalian, et al., Mechanisms and kinetics of methane thermal conversion in a syngas, Ind. Eng. Chem. Res. 48 (2009) 6564–6572, https://doi.org/10.1021/ie900343b.
[54] G. Schuster, G. Löffler, K. Weigl, H. Hofbauer, Biomass steam gasification – an extensive parametric modeling study, Bioresour. Technol. 77 (2001) 71–79, https://doi.org/10.1016/S0960-8524(00)00115-2.
[55] Spath P., Aden A., Eggeman T., Ringer M., Wallace B., Jechura J. Biomass to hydrogen production detailed design and economics utilizing the battelle columbus laboratory indirectly-heated gasifier. 2005. https://doi.org/10.2172/15016221.
[56] L. Abdelouahed, O. Authier, G. Mauviel, J.P. Corriou, G. Verdier, A. Dufour, Detailed modeling of biomass gasification in dual fluidized bed reactors under Aspen plus, Energy Fuels 26 (2012) 3840–3855, https://doi.org/10.1021/ef300411k.
[57] K.Y. Kwong, E.J. Marek, Combustion of biomass in fluidized beds: a review of key phenomena and future perspectives, Energy Fuels 35 (2021) 16303–16334, https://doi.org/10.1021/acs.energyfuels.1c01947.
[58] K.Y. Kwong, R. Mao, S.A. Scott, J.S. Dennis, E.J. Marek, Analysis of the rate of combustion of biomass char in a fluidised bed of CLOU particles, Chem. Eng. J. 417 (2021) 127942, https://doi.org/10.1016/j.cej.2020.127942.
[59] M. Morin, S. Pécate, M. Hémati, Kinetic study of biomass char combustion in a low temperature fluidized bed reactor, Chem. Eng. J. 331 (2018) 265–277, https://doi.org/10.1016/j.cej.2017.08.063.
[60] K.-M. Hansson, J. Samuelsson, C. Tullin, L.-E. Åmand, Formation of HNCO, HCN, and NH3 from the pyrolysis of bark and nitrogen-containing model compounds, Combust. Flame 137 (2004) 265–277, https://doi.org/10.1016/j.combustflame.2004.01.005.
[61] J.-P. Cao, L.-Y. Li, K. Morishita, X.-B. Xiao, X.-Y. Zhao, X.-Y. Wei, et al., Nitrogen transformations during fast pyrolysis of sewage sludge, Fuel 104 (2013) 1–6, https://doi.org/10.1016/j.fuel.2010.08.015.
[62] S. Kambara, T. Takarada, Y. Yamamoto, K. Kato, Relation between functional forms of coal nitrogen and formation of nitrogen oxide (NOx) precursors during rapid pyrolysis, Energy Fuels 7 (1993) 1013–1020, https://doi.org/10.1021/ef00042a045.
[63] F.-J. Tian, J. Yu, L.J. McKenzie, J. Hayashi, C.-Z. Li, Conversion of fuel-N into HCN and NH3 during the pyrolysis and gasification in steam: a comparative study of coal and biomass, Energy Fuels 21 (2007) 517–521, https://doi.org/10.1021/ef060415r.
[64] A. Stagni, C. Cavallotti, S. Arunthanayothin, Y. Song, O. Herbinet, F. Battin-Leclerc, et al., An experimental, theoretical and kinetic-modeling study of the gas-phase oxidation of ammonia, React. Chem. Eng. 5 (2020) 696–711, https://doi.org/10.1039/C9RE00429G.
[65] H. Li, M. Li, H. Wang, M. Tan, G. Zhang, Z. Huang, et al., A review on migration and transformation of nitrogen during sewage sludge thermochemical treatment: focusing on pyrolysis, gasification and combustion, Fuel Process. Technol. 240 (2023) 107562, https://doi.org/10.1016/j.fuproc.2022.107562.
[66] A. Anca-Couce, P. Sommersacher, N. Evic, R. Mehrabian, R. Scharler, Experiments and modelling of NOx precursors release (NH3 and HCN) in fixed-bed biomass combustion conditions, Fuel 222 (2018) 529–537, https://doi.org/10.1016/j.fuel.2018.03.003.
[67] H. Chen, R. Shan, F. Zhao, J. Gu, Y. Zhang, H. Yuan, et al., A review on the NOx precursors release during biomass pyrolysis, Chem. Eng. J. 451 (2023) 138979, https://doi.org/10.1016/j.cej.2022.138979.
[68] Z. Wang, J. Shen, X. Liu, Y. Guo, S. Wang, S. Deng, et al., A review on nitrogen migration mechanism during the pyrolysis of organic solid waste: DFT, ReaxFF MD and experimental study, J. Anal. Appl. Pyrolysis 176 (2023) 106250, https://doi.org/10.1016/j.jaap.2023.106250.
[69] W.R. Johnson, J.C. Kan, Mechanisms of hydrogen cyanide formation from the pyrolysis of amino acids and related compounds, J. Org. Chem. 36 (1971) 189–192, https://doi.org/10.1021/jo00800a038.
[70] R.J. Evans, T.A. Milne, Molecular characterization of the pyrolysis of biomass, Energy Fuels 1 (1987) 123–137, https://doi.org/10.1021/ef00002a001.
[71] D.L. Carpenter, R.L. Bain, R.E. Davis, A. Dutta, C.J. Feik, K.R. Gaston, et al., Pilot-scale gasification of corn stover, switchgrass, wheat straw, and wood: 1. Parametric study and comparison with literature, Ind. Eng. Chem. Res 49 (2010) 1859–1871, https://doi.org/10.1021/ie900595m.
[72] M. Nowakowska, O. Herbinet, A. Dufour, P.-A. Glaude, Detailed kinetic study of anisole pyrolysis and oxidation to understand tar formation during biomass combustion and gasification, Combust. Flame 161 (2014) 1474–1488, https://doi.org/10.1016/j.combustflame.2013.11.024.
[73] S. Chiaberge, I. Leonardis, T. Fiorani, P. Cesti, S. Reale, F.D. Angelis, Bio-oil from waste: a comprehensive analytical study by soft-ionization FTICR mass spectrometry, Energy Fuels 28 (2014) 2019–2026, https://doi.org/10.1021/ef402452f.
[74] Y. Kostyukevich, M. Vlaskin, L. Borisova, A. Zherebker, I. Perminova, A. Kononikhin, et al., Investigation of bio-oil produced by hydrothermal liquefaction of food waste using ultrahigh resolution Fourier transform ion cyclotron resonance mass spectrometry, Eur. J. Mass Spectrom. 24 (2018) 116–123, https://doi.org/10.1177/1469066717737904.
[75] T. Kekäläinen, T. Venäläinen, J. Jänis, Characterization of Birch wood pyrolysis oils by ultrahigh-resolution fourier transform ion cyclotron resonance mass spectrometry: insights into thermochemical conversion, Energy Fuels 28 (2014) 4596–4602, https://doi.org/10.1021/ef500849z.
[76] N.S. Tessarolo, R.V.S. Silva, G. Vanini, A. Casilli, V.L. Ximenes, F.L. Mendes, et al., Characterization of thermal and catalytic pyrolysis bio-oils by high-resolution techniques: ^{1}H NMR, GC×GC-TOFMS and FT-ICR MS, J. Anal. Appl. Pyrolysis 117 (2016) 257–267, https://doi.org/10.1016/j.jaap.2015.11.007.
[77] J. Hertzog, V. Carré, Y. Le Brech, C.L. Mackay, A. Dufour, O. Mašek, et al., Combination of electrospray ionization, atmospheric pressure photoionization and laser desorption ionization Fourier transform ion cyclotronic resonance mass spectrometry for the investigation of complex mixtures – application to the petroleomic analysis of bio-oils, Anal. Chim. Acta 969 (2017) 26–34, https://doi.org/10.1016/j.aca.2017.03.022.
[78] W. Jablonski, K.R. Gaston, M.R. Nimlos, D.L. Carpenter, C.J. Feik, S.D. Phillips, Pilot-scale gasification of corn stover, switchgrass, wheat straw, and wood: 2. identification of global chemistry using multivariate curve resolution techniques, Ind. Eng. Chem. Res. 48 (2009) 10691–10701, https://doi.org/10.1021/ie900596v.